Characterization and Analysis of Low Room Temperature Ductility Nickel-Based Superalloy 718 Plus for Aircraft Engine Forgings

Jonathon Bracci

June 2012

Prof. Blair London Advisor

Materials Engineering Department

California Polytechnic State University, San Luis Obispo

Approval Page

Project Title: Characterization and Analysis of Low Room Temperature Ductility Nickel-Based Superalloy 718 Plus for Aircraft Engine Forgings

Author: Jonathon Bracci

Date Submitted: June 1, 2012

CAL POLY STATE UNIVERSITY
Materials Engineering Department

Since this project is a result of a class assignment, it has been graded and accepted as fulfillment of the course requirements. Acceptance does not imply technical accuracy or reliability. Any use of the information in this report, including numerical data, is done at the risk of the user. These risks may include catastrophic failure of the device or infringement of patent or copyright laws. The students, faculty, and staff of Cal Poly State University, San Luis Obispo cannot be held liable for any misuse of the project.

Prof. Blair London
Faculty Advisor

_____
Signature

Prof. Trevor Harding
Department Chair

_____
Signature

Abstract

Schlosser Forge Co. forges low pressure turbine (LPT) cases from the nickel based superalloy 718 Plus using the ring rolling forging process. Schlosser has been experiencing low room temperature ductility problems in a number of their 718 Plus LPT cases. LPT cases are required to pass a 4D tensile test at room temperature with a minimum of 15 percent elongation. The ductility problem was reduced by increasing the forging temperature from 1825˚F to 1850˚F. Analysis was performed on 718 Plus samples taken from forged LPT cases that failed the room temperature ductility requirement and ones that passed the requirement. The analysis required conducting grain size measurements and delta phase volume fraction measurements to relate these microstructural characteristics to low room temperature ductility. Samples of 718 Plus were mounted and polished for metallography in accordance with ASTM E3-11. Samples were etched with modified Kalling's reagent for 3 minutes and grain size measurements were taken per ASTM E112-10. Grain sizes varied only slightly between the low and acceptable ductility samples, with an average grain diameter of 44.9 μm. Grain size variation was not contributing to the low room temperature ductility problem. The samples were then re-polished to remove the previous etch and re-etched with modified Kalling's for 30 seconds. The 30 second etch allowed the delta phase precipitates to be revealed while leaving the grain boundaries un-etched. Volume fraction measurements of the delta phase precipitates were taken per ASTM E562-11. Results showed the low ductility sample contained the highest amount of delta, about 7.5 percent by volume. The amount of delta was found to be inversely proportional to ductility as well as forging temperature.

Keywords: Materials Engineering, Superalloys, Forging, Ring Rolling, 718 Plus, Delta Phase, Grain Size

Table of Contents

List of Figures

List of Tables

Introduction

Problem Statement

Schlosser Forge Co. (Rancho Cucamonga, CA) forges seamless rings from nickel-based superalloys for use in aircraft turbine engines. One type of seamless ring forged at Schlosser is a low pressure turbine (LPT) case that forms the housing around the low pressure turbine blades in an aircraft engine. LPT cases are forged out of a new nickel-based superalloy called 718 Plus. Once forging of a LPT case is completed, test samples from the case are mechanically tested to ensure each case has the required mechanical properties. Schlosser is encountering a problem with some of their LPT cases exhibiting low ductility at room temperature. Each LPT case is required to have a minimum of 15 percent elongation at room temperature and cases that do not pass this test are considered defective. Recently, the ductility problem has been reduced by increasing the LPT case forging temperature from 1825˚F to 1850˚F. The significance being the higher forging temperature is now above the δ phase solvus temperature. It is important to characterize the microstructures of low ductility and acceptable ductility cases to prevent further room temperature ductility problems. Characterization of the 718 Plus microstructure will be done by determining grain sizes and volume fractions of δ phase precipitates. The microstructural analysis of 718 Plus samples should allow for relationships to be established between microstructural characteristics, room temperature ductility, and forging temperature. These relationships will help Schlosser better understand the low ductility problem and allow them to alter their forging process to eliminate the problem.

Nickel-Based Superalloys

Background

In order to understand the effects that microstructure has on room temperature ductility in 718 Plus it is important to first have a general knowledge of nickel-based superalloys. Nickel-based superalloys were first developed in the early 1940s. With the development of the jet engine, a new type of alloy was

needed that could withstand the high temperatures subjected to jet engine components. This led to the development of nickel-based superalloys. A superalloy, by definition, is an alloy rich in at least one of the elements nickel, cobalt, titanium, niobium, or iron and maintains structural, surface and property stability at elevated temperatures, under high stress, and in severe environments[1]. Today superalloys have a wide range of applications, but the majority of superalloys, including nickel-based, are used in the aircraft gas turbine engine industry (Figure 1). There are over 100 different types of nickel-based superalloys in existence and are primarily utilized in the wrought or cast form.

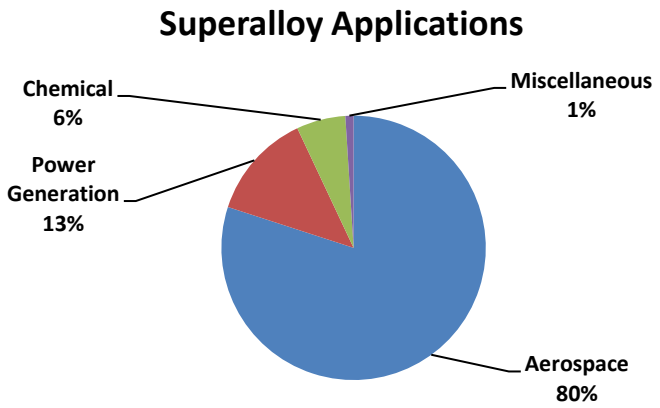

Figure 1. Applications of today's superalloys and their distributions. The vast majority of applications are for aerospace.[1]

Physical Metallurgy

Nickel-based superalloys consist of a number of different alloying elements, each one contributing to the strength of the alloy. Of these different alloying elements, the most common are: chromium, cobalt, titanium, molybdenum, tungsten, aluminum, and niobium (Table I). Together, these elements provide two types of strengthening mechanisms: solid solution strengthening and precipitation strengthening. The latter is the most predominant in nickel-based superalloys. The microstructure of nickel-based superalloys consists of an austenitic FCC structured matrix known as the γ phase. The γ matrix is strengthened by solid solution elements such as chromium, cobalt, tungsten, molybdenum, and aluminum. Tungsten, chromium, and molybdenum are the strongest solid solution strengtheners and differ from nickel in atomic diameter by about 3 to 13 percent[2]. There are also a number of intermetallic precipitates

dispersed in the γ matrix and along grain boundaries. While solid solution strengthening is present in these alloys, precipitation hardening is responsible for the primary source of strength. These precipitates include the γ′ FCC ordered $Ni_3(Al,Ti)$ phase, γ″ BCT ordered Ni_3Nb phase, δ orthorhombic Ni_3Nb phase, and η BCT ordered Ni_3Ti phase. Also present in the microstructure are a number of different carbides, including MC, $M_{23}C_6$, and M_6C where the M stands for a metallic element.

Table I. Ranges of Common Alloying Elements in Superalloys.[3]

Element	Range, %	
	Fe-Ni- and Ni-base	Co-base
Cr	5-25	19-30
Mo, W	0-12	0-11
Al	0-6	0-4.5
Ti	0-6	0-4
Co	0-20	. . .
Ni	. . .	0-22
Nb	0-5	0-4
Ta	0-12	0-9
Re	0-6	0-2

Gamma Prime

The γ′ phase has an FCC ordered structure with the composition of either Ni_3Al or Ni_3Ti. The precipitation of γ′ in the γ matrix is responsible for giving most nickel-based superalloys their primary source of strength; with the exception of Inconel 718 which is strengthen by γ″ precipitates. Strength from γ′ precipitates can be directly correlated to the volume fraction and size of the γ′ particles. At peak aged condition, the γ′ particles are coherent with the γ matrix and are between 0.25 to 0.50 μm in size. Peak aged strength arises from dislocations having to shear though the γ′ particles (Figure 2). Over aging of the superalloy will cause γ′ particles to coarsen, becoming incoherent with the γ matrix and eventually leading to the formation of either δ or η secondary intermetallic phases. The coarsening of the γ′ leads to a decrease in strength due to dislocations now bowing around particles. Along with size, volume fraction of γ′ precipitates also has a strong effect on strength. An increase in strength is directly proportional to an

increase in the volume fraction of γ′ precipitates (Figure 3). The structure of γ′ particles can be either spheroidal or cuboidal in shape depending on the volume fraction of γ′ (Figure 4). In alloys like Waspaloy that have lower volume fractions of γ′, approximately 30 percent, the γ′ particles will be spherical in shape. In alloys with higher volume fractions of γ′ between 40 and 45 percent, like Udimet 700, particles will be cube shaped. To achieve the peak age condition, most nickel-based superalloys are solution treated at a temperature above the γ′ solvus temperature and then age hardened in one or more age hardening heat treatments.

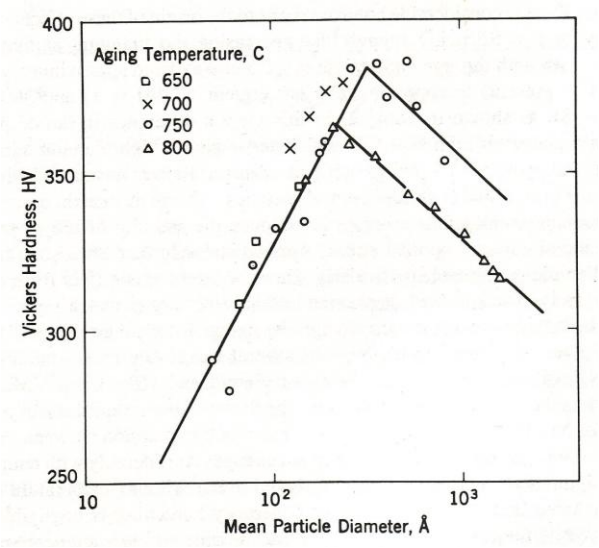

Figure 2. Hardness verse size of γ′ particles in a nickel-based superalloy showing the effect that particles size has on strength.[4]

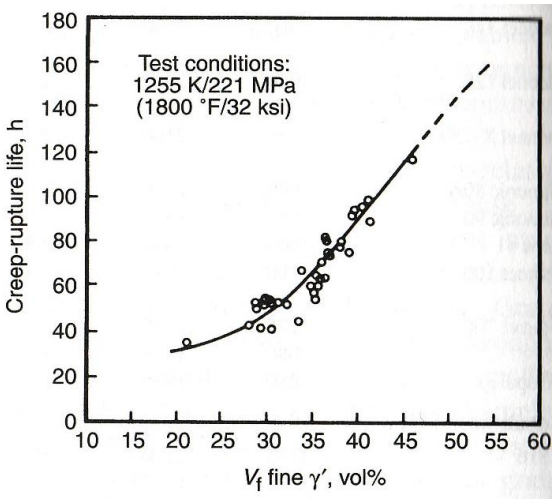

Figure 3. Creep-rupture life verses V_f of γ′ showing that an increase in strength is directly related an increase in the V_f of γ′ particles.[5]

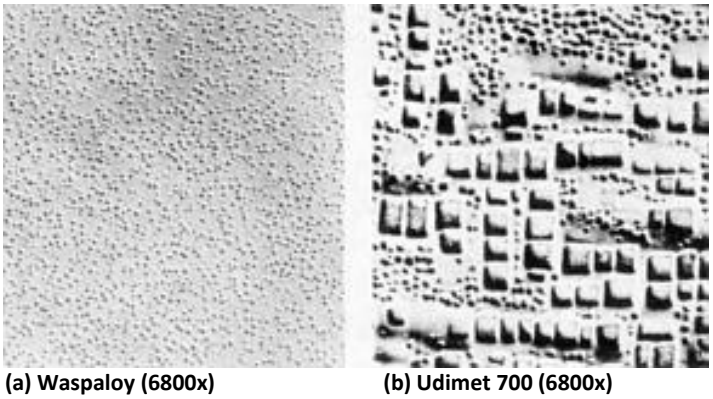

(a) Waspaloy (6800x) **(b) Udimet 700 (6800x)**

Figure 4. Spherical shape of γ′ particles in superalloys with a low V_f of γ′ (Waspaloy left) and cubical shape of γ′ particles in alloys with a high V_f of γ′ (Udimet 700 right).[5]

Gamma Double Prime

The γ″ phase has a BCT ordered structure with the composition of Ni_3Nb. Like γ′, particles of γ″ also precipitate out into the γ matrix and provide strength. Most nickel-based superalloys are strengthened by γ′ precipitates but small amounts of γ″ precipitates can also be present. An exception to this is Inconel 718, a nickel-based superalloy where γ″ precipitates are the predominant strengthening mechanism. The use of γ″ particles as a strengthening mechanism is usually limited to nickel-based superalloys that contain niobium in excess of 4 weight percent, like Inconel 718[6]. The relationship between γ″ and the mechanical properties of nickel-based superalloys has not been extensively studied compared to γ′ so not as much information is known. One similarity between γ′ and γ″ particles is that the volume fraction of γ″ particles is also proportional to the strength of the superalloy. After this the similarities end. Unlike γ′, γ″ particles are disk like in shape and are not stable, tending do dissolve back into the matrix at low temperatures. Also, there is no relationship between γ″ particles size and strength like there is with γ′. The most important characteristic of γ″ is the ease with which it forms after the solution heat treatment. This allows for γ″ hardened alloys to be easily aged to peak conditions after welding or other thermal processing treatments. The γ″ phase as mentioned before is not normally stable and will tend to convert to γ′ and δ with exposure to moderate temperatures (greater than 1250˚F) for long periods of time. This can result in precipitate-free zones (PFZ) which will cause a reduction in notch ductility and lead to a reduction in the alloy's strength[6].

Carbides

Carbides, like γ′ and γ″ precipitates, also play an important role in strengthening nickel-based superalloys. The formation of carbides is the result of carbon content in the alloy. For wrought nickel-based superalloys, carbon contents can vary between 0.02 to 0.2 percent and can be as high as 0.6 percent in cast alloys[7]. Carbides form along grain boundaries and within grains. Carbides that form along grain boundaries have the strongest influence on mechanical properties. The most common types of carbides that form are MC, $M_{23}C_6$, and M_6C where the M stands for a metallic element such as chromium,

titanium, tungsten or niobium. In most nickel-based superalloys, $Cr_{23}C_6$ carbides form along the grain boundaries. There exists an optimum distribution of carbides along grain boundaries which will result in the best mechanical properties. The absence of carbides along grain boundaries can lead to the formation of voids during high temperature deformation and to premature failure of the alloy. This is because grain boundary movement is unrestricted and will result in low creep resistance and cracking at grain boundary triple points. The other extreme is a continuous film of carbides along grain boundaries. A film of carbides will prevent grain boundaries from sliding and lead to excessive stress build up and premature failure. Also, because carbides are brittle they are more susceptible to cracking, so continuous films of carbides can severely reduce impact toughness of the alloy. An excess amount of carbides along grain boundaries can also result in PFZs of γ' on either side of the grain boundary. These PFZs can lead to low stress rupture properties and cause premature failure due to a high buildup of dislocations in these zones. The optimum condition exists when discontinuous carbide particles form along grain boundaries (Figure 5). The discontinuous chains of carbides help to hinder grain boundary sliding while providing enough ductility for stress relaxation to occur without premature failure. It is therefore important to achieve the optimum distribution of carbides along grain boundaries to maintain good creep resistance and stress rupture life in the alloy.

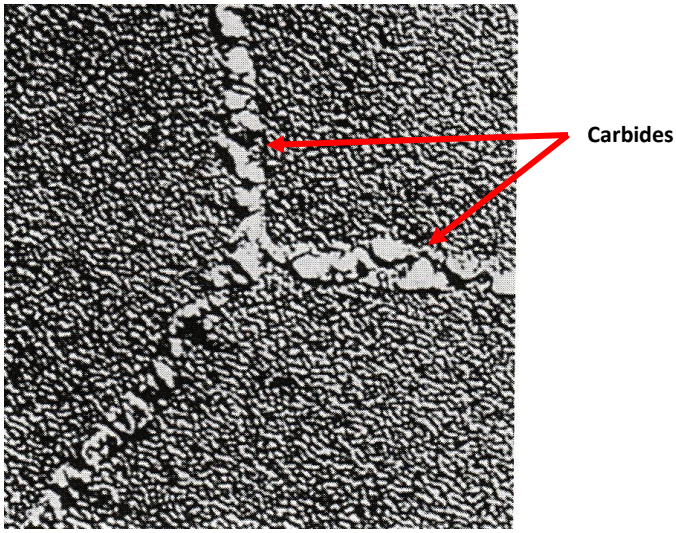

Figure 5. Discontinuous carbide precipitation along grain boundaries in Waspaloy.[8] (10,000x)

Grain Size:

Grain size in nickel-based superalloys is also an important factor influencing mechanical properties. Most commonly, grain sizes are measured using ASTM standards, specifically ASTM E112-01. Grain size can be correlated to an ASTM grain size number *G* (Table II), and is calculated using the ASTM grain size equation where *n* is the number of grain per square inch at 100x magnification (Equation 1).

$$n = 2^{G-1} \quad \textbf{(Eq 1)}$$

In general, fine grains result in good room temperature properties such as toughness, strength and fatigue resistance. Coarser grain sizes will provide better creep resistance at elevated temperatures but will reduce other properties that benefit from finer grain sizes. Also, coarser grain structures result in fewer amounts of grain boundaries. This causes carbides to become more concentrated at grain boundaries and can result in the formation of continuous carbide films. As mentioned previously, a continuous film of carbides along grain boundaries can be detrimental to the mechanical properties of nickel-based superalloys. Another condition that can occur is duplex grain structures. A duplex grain structure is one where multiple grain sizes exist in the alloy. Properties can vary between regions with different sized grains making it difficult to achieve uniformity. Premature failure of an alloy with duplex grains can occur in a region where undesirable properties exist as a result of different grain sizes.

Table II. ASTM Grain Size Number Correlated to Average Grain Diameter[9]

ASTM Grain Size Number	Average Grain Diameter (μm)
3	127.0
4	89.8
5	63.5
6	44.9
7	31.8
8	22.5

Secondary Intermetallic Phases

The formation of secondary intermetallic phases occurs when the alloy is exposed to elevated temperatures for long periods of time. These phase include η, δ, σ, and Laves. The η and δ phases have been mentioned previously and are formed from the coarsening of either γ′ or γ″ precipitates. The size and shape of both η and δ phases are less effective in strengthening the alloy compared to fine γ′ and γ″ precipitates. Precipitation of η and δ phases usually occurs along grain boundaries as cellular products or intragranularly as Widmanstätten plates. Large volume fractions of η and δ are associated with reduced mechanical properties due to their coarse structure and the consumption of γ′ and γ″ precipitates. The formation of σ and Laves phases also has a negative effect on mechanical properties of the alloy. The σ phase is a tetragonal close packed ordered phase and can form as plates or grain boundary films. Excess amount of σ has been shown to reduce stress rupture life of the alloy (Figure 6). The Laves phase is also a TCP ordered phase and has the general formula $(Fe,Cr,Mn,Si)_2(Mo,Ti,Nb)$. Laves phase commonly form as coarse intragranular particles and have the effect of lowering the room temperature ductility of the alloy. The formation of both σ and Laves phased can be controlled by reducing the number of electron vacancies in the base metal and by controlling heat treatment times and temperatures[10]. The number of election vacancies can be reduced by controlling the composition of the alloy.

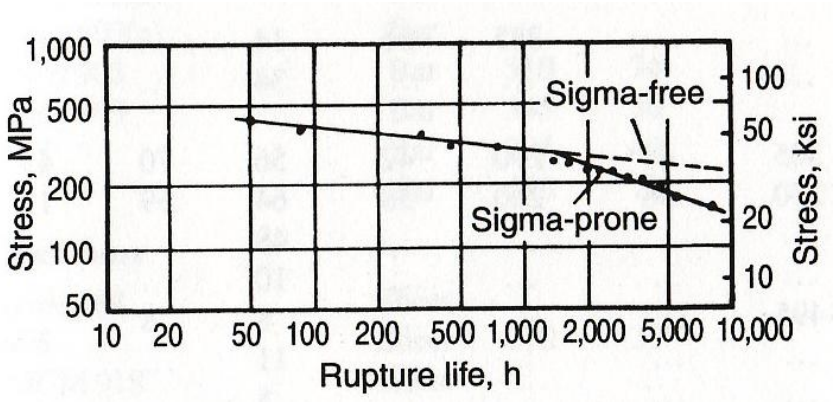

Figure 6. Stress rupture properties of Udimet 700 showing a reduction in stress rupture strength with the formation of σ phase.[10]

718 Plus Alloy

ATI Allvac (Monroe, NC) has recently developed a new nickel-based superalloy called 718 Plus. The purpose of 718 Plus is to replace two existing nickel-based superalloys: Inconel 718 and Waspaloy. 718 Plus exhibits the superior formability of Inconel 718 while retaining the high temperature strength and stability properties of Waspaloy (Figure 7). The alloy is also less expensive than Waspaloy and other high temperature nickel-based superalloys due to lower raw material costs. Typically, 718 Plus is used in

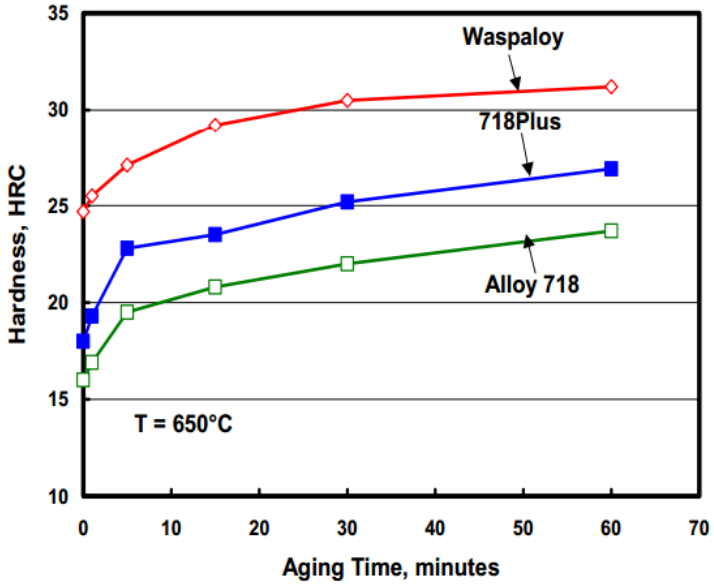

Figure 7. Aging time vs. hardness plot comparing 718 Plus to Waspaloy and Inconel 718. (704˚C aging temperature)[11]

non-rotating components of gas turbine engines, such as cases or rings. Schlosser Forge Co. forges 718 Plus LPT cases which are used in the new General Electric 90 series aircraft engines (Figure 8). Like most nickel-based superalloys, 718 Plus is comprised of an austenitic γ matrix that is precipitation hardened by FCC ordered $Ni_3(Al,Ti,Nb)$ γ′ particles. Unlike Waspaloy and other γ′ strengthened alloys, the γ′ precipitates in 718 Plus are rich in Nb and Al. The typical volume fraction of γ′ precipitates in 718 Plus varies from 19 to 23 percent. Small amounts of γ″ precipitates can also be present in the microstructure, usually less than 7 percent[12]. The γ′ phase is much more stable at high temperature compared to γ″.

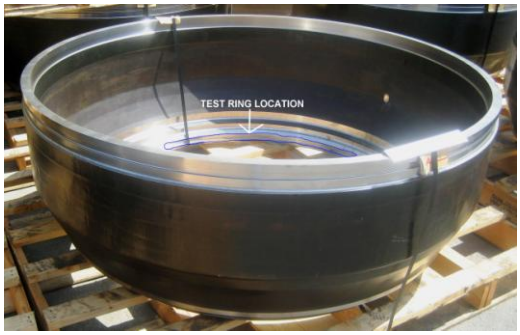

Figure 8. 718 Plus low pressure turbine case forged at Schlosser Forge Co. (Image provided by Schlosser Forge Co.)

Because 718 Plus is primarily strengthened by γ′ it has better thermal stability, up to about 1400˚F, over γ″ strengthened alloys like Inconel 718. Grain boundaries in 718 Plus are strengthened by Ni_3Nb δ phase precipitates as well as small amounts of NbC carbides. The volume fraction of δ phase in 718 Plus is usually between 5 and 10 percent and is important in providing good stress rupture and notch ductility properties[12]. The solvus temperature of δ is 1830˚F and the formation of δ phase precipitates occurs during forging and subsequent heat treatments. Studies have shown that δ phase precipitation first occurs on grain boundaries, then twin boundaries, and finally within grains (Figure 9). The δ phase precipitate amount has a strong effect on the mechanical properties of 718 Plus. There exists an optimum volume fraction and morphology of δ phase precipitates which will provide the best possible mechanical properties. The distribution of nearly continuous, short rod shaped δ phase precipitates along grain boundaries have been shown to provide the best mechanical properties (Figure 10)[13]. Mechanical properties can be severally reduced with excessive δ phase precipitation along grain boundaries, twin boundaries and intragranularly which can lead to low tensile and stress rupture strength. Excessive amounts of δ phase precipitates can occur as a result of long heat treatment times. In contrast, too few δ phase precipitates can also degrade mechanical properties leading to low strength and premature stress rupture failure. Little to no δ delta phase precipitates can result from excessive forging and heat treatment temperatures.

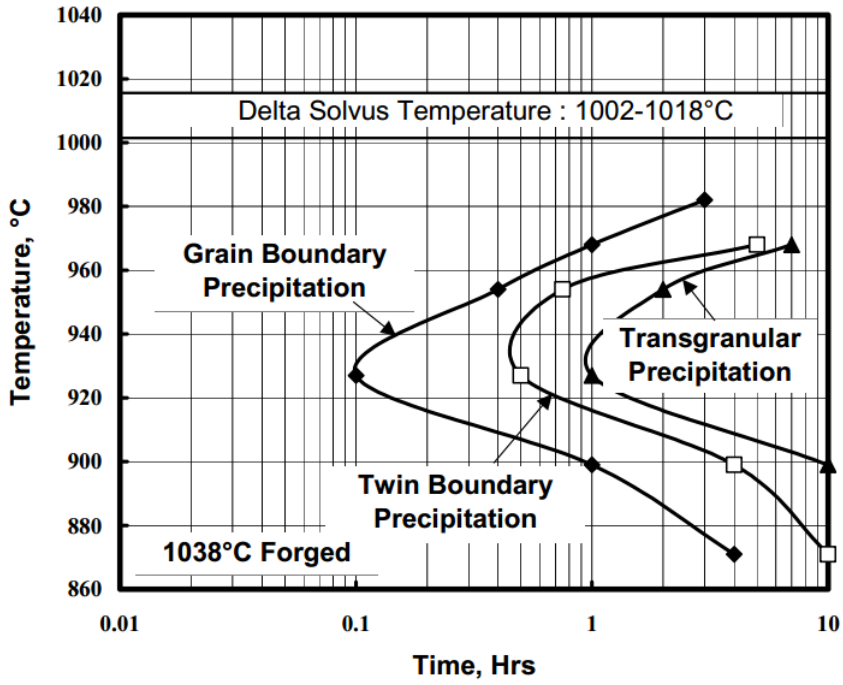

Figure 9. Experimentally determined TTT diagram of δ phase precipitation in 718 Plus.[11]

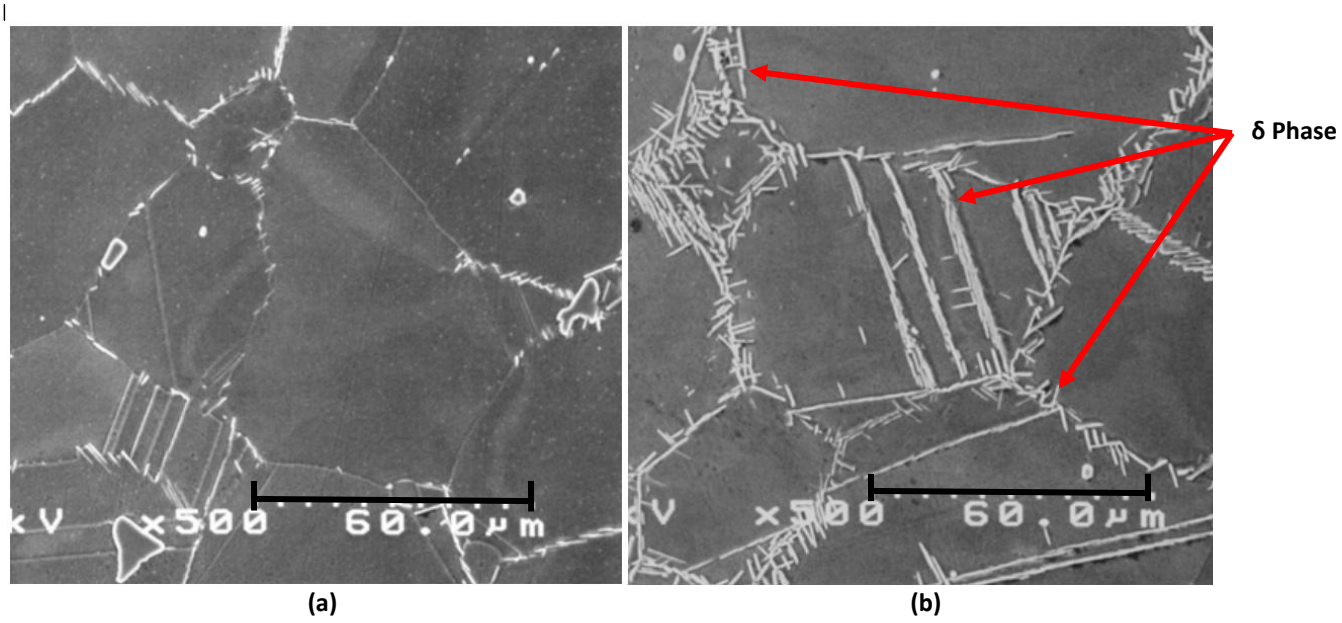

Figure 10. SEM images of 718 Plus with optimum volume fraction and morphology of δ phase precipitates along grain boundaries (a) and excessive amounts of δ phase precipitates at grain boundaries and twin boundaries (b).[13]

Ring Rolling Forging Process

The forging process used to produce seamless ring is called ring rolling (Figure 11). Schlosser Forge Co. uses ring rolling to forge 718 Plus LPT cases. Ring rolling starts out with a perform of material in the shape of a doughnut. At Schlosser, 718 Plus preforms are heated to between 1825˚F and 1850˚F during forging. The doughnut shaped preform is placed over a mandrel with a diameter slightly smaller than the hole in the preform. Then a second mandrel is brought up against the preform and applies pressure, squeezing the preform against the first mandrel. Next, the second mandrel begins to rotate causing the preform to rotate. As the preform rotates, force from the outside mandrel is constantly applied reducing the preform's thickness, increasing its diameter. While the preform is rotated, axial rollers contact the top and bottom of the preform to control its height. The result of the ring rolling process yields a seamless ring (Figure 12). Rings can either be uniform with a rectangular cross section, or contoured with flanges or grooves. To get to its final shape, a preform usually will go through multiple ring rolling steps. During each step, the diameter will be increased and the cross sectional geometry will become more refined. The size and complexity of the cross sectional geometry will determine the number of steps used in the ring rolling process.

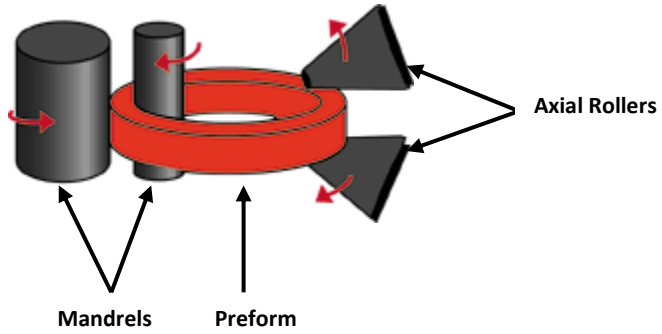

Figure 11. Diagram of the ring rolling process showing how a seamless ring is rolled.[14]

Figure 12. Ring rolling process in action with a red hot preform being forged.[15]

Experimental Procedure

Sample Preparation

The first step in characterizing the microstructure of 718 Plus LPT cases was to prepare samples for metallography in accordance with ASTM E3-11[16]. A total of three test rings taken from 718 Plus LPT cases were provided by Schlosser Forge. Two of the test rings came from LPT cases forged at 1825˚F. Of these rings, one was taken from a LPT case that failed the room temperature ductility requirement and the other from a case that passed the requirement. The third test ring came from a LPT case forged at 1850˚F that also passed the room temperature ductility requirement. Two samples of 718 Plus were cut from each test ring for a total of six samples (Table III). Samples were cut using an abrasive cut-off saw cooled by cutting fluid. The cutting fluid ensured the heat generated during the cutting process would not alter any microstructural characteristics in the samples. Next, samples were mounted in Diallyl Phthalate powder (Figure 13). One sample per ring was oriented in the transverse direction and the other in the longitudinal direction. This allowed samples to be viewed from two orientations per test ring. Once mounted, samples were abraded with progressively finer SiC paper up to 600 grit. Between each grit, samples were rotated 90 degrees. Each sample was then polished with 6 μm diamond polish and a final polish of 1 μm diamond.

Table III. Samples Prepared for Microstructural Analysis

Forging Temperature	Ductility	Samples Examined
1825°F	Low	2
1825°F	High	2
1850°F	High	2

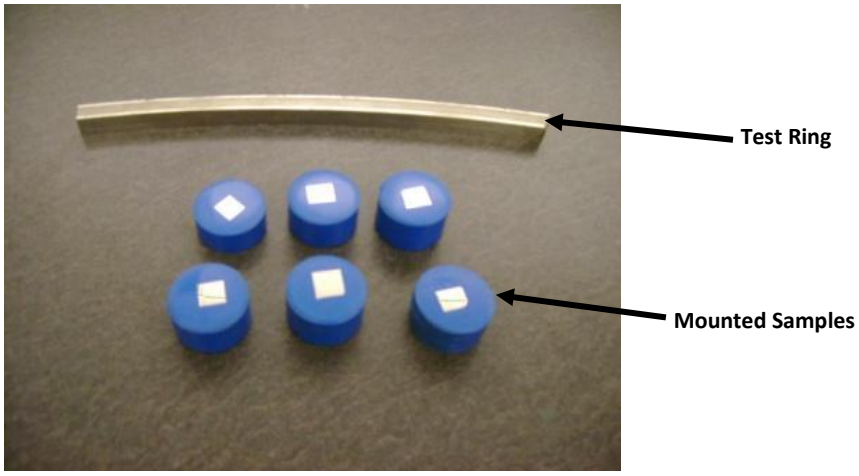

Figure 13. Portion of a test ring cut from a 718 Plus LPT case and samples mounted in Diallyl Phthalate. Samples were cut from test rings like the one shown.

Grain Size Measurements

After each sample had undergone final polishing, they were etched in preparation for grain size analysis. Problems were encountered with finding the correct etch and etch time that would clearly reveal grain boundaries in the microstructure. Upon further research and experimentation it was determined that etching the samples for three minutes using a modified Kalling's etch produced the best results. The etch revealed grain boundaries along with δ phase precipitates and some carbides (Figure 14). Grain sizes of each sample were measured using two methods. The first method utilized a software program called IQMaterials (IQM) that automatically measured grain sizes in a micrograph. The second method was to manually measure grain sizes. Results could then be compared to see how grain size varied between low and acceptable ductility samples as well as between the two grain size measurement methods.

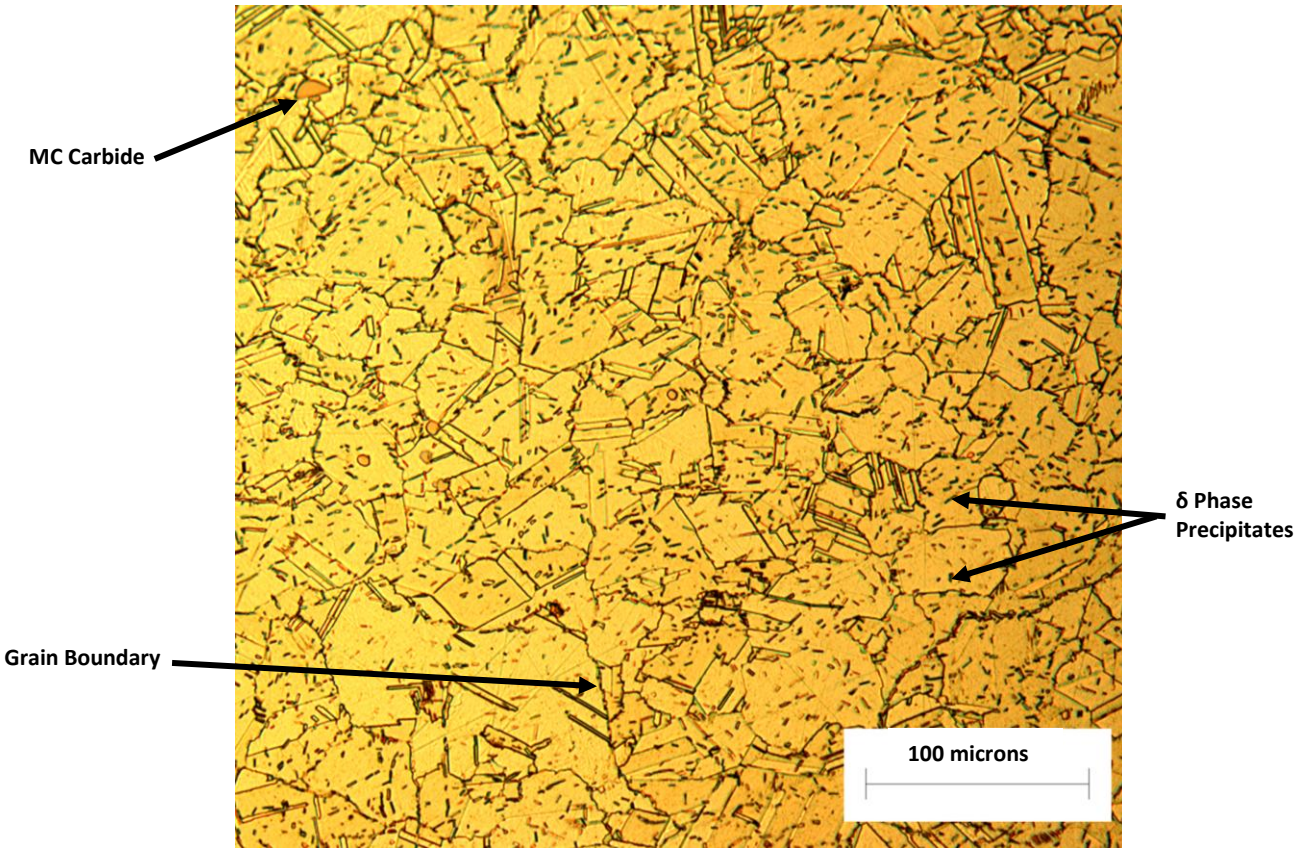

Figure 14. Micrograph of a 718 Plus sample used for grain size measurements showing grain boundaries, δ phase precipitates, and carbides. Modified Kalling's, 200x

Automated Grain Size Measurements

Automated grain size measurements were performed in accordance with ASTM E1382-97[17]. Five micrographs per sample were produced: one from the middle and four from each of the four corner of the sample, all at 200x magnification. Then, each micrograph was analyzed using the IQM program. The program superimposed three concentric circular test lines of a known total length of 2.919 mm onto each micrograph (Figure 15). The program then counted the number of grain boundaries intersected by the three circular test lines and using this number calculated the ASTM grain size number G. The grain size in each micrograph was measured using the same technique and program settings to minimize variation in the data. Five grain size numbers were acquired per sample and then averaged to get the mean grain size for the entire sample.

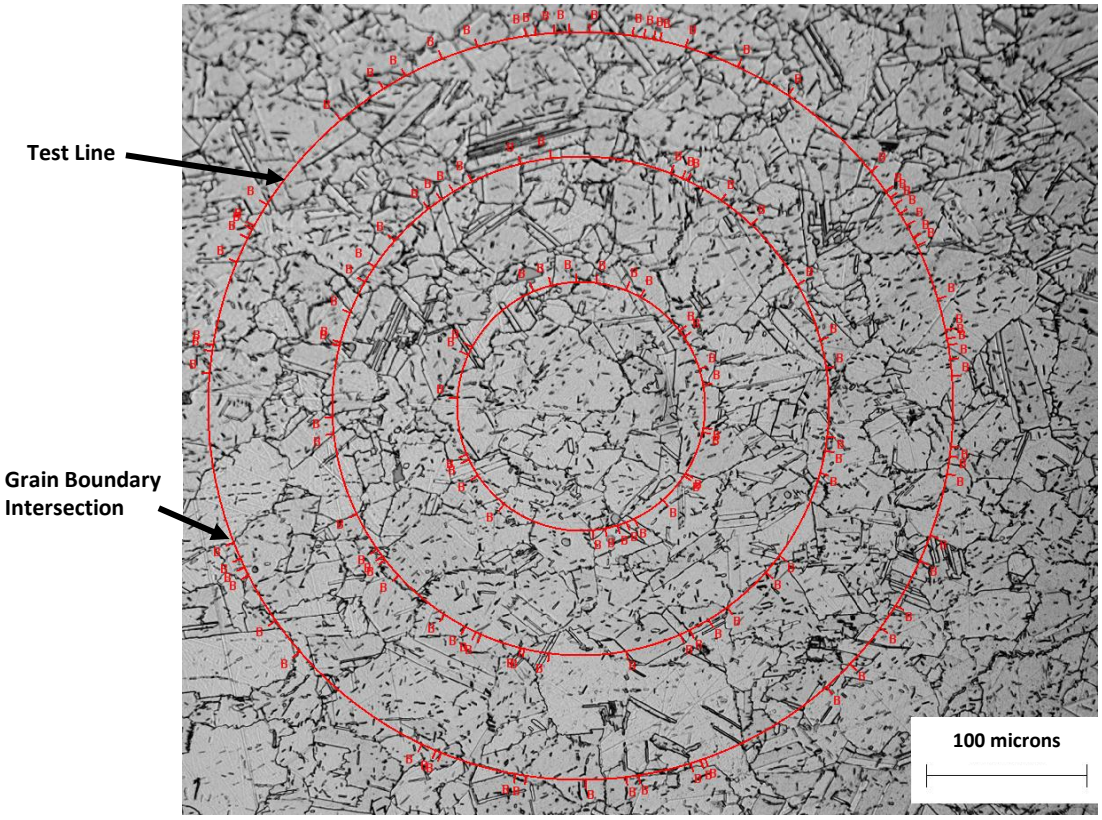

Figure 15. IQMaterials program measuring grain size in a 718 Plus micrograph showing the circular test lines and grain boundary intersection points determined by the program. Note a number of precipitates have been marked as grain boundaries. Modified Kalling's, 200x

A problem was encountered in using the IQM program to measure grain size. The 718 Plus microstructure contained grain boundaries and δ phase precipitates. In the micrographs, the precipitates have similar color and contrast to the grain boundaries. This posed a problem because the software program has no way of distinguishing between grain boundaries and precipitates. Thus, the program frequently counted precipitates as grain boundaries. This problem caused the calculated ASTM grain sizes numbers to be greater than they actually were for each sample. To overcome this problem, grain sizes were measured by counting the number of grain boundary intersections by a manual method.

Manual Grain Size Measurements

Manual grain size measurements were conducted per ASTM E112-10[9]. By using this method, the problem encountered with the automated grain size measurement method was eliminated. The same set of 718 Plus micrographs was used in the manual grain size measurement procedure. The IQM program was used again to superimpose the circular test lines onto the micrographs. Then, the number of grain boundary intersections per micrograph was counted by hand. The total number of grain boundary intersections was then divided by the total test line length, 2.919 mm, which gave the number of grain boundary intercepts per unit length (P_{Li}). This number could then be plugged into the equation provided in the ASTM standard to get the ASTM grain size number G. This method was repeated for all six samples.

Delta Phase Volume Fraction Measurements

The volume fraction of δ phase precipitates was measured next. To prepare for volume fraction measurements, each sample was re-polished to remove the etch used for grain size measurements. Samples were then etched again with modified Kalling's and etch time was reduced to 30 seconds. The shortened etch time allowed only δ phase precipitates to be revealed in the microstructures while leaving grain boundaries un-etched (Figure 16). This was important to facilitate the measurement of only the volume fraction of δ because grain boundaries could not be mistaken for δ phase precipitates. Like the grain size measurements, two methods were again used to measure the volume fraction of δ in each sample. The first method used the IQM program once more to automatically measure volume fractions of δ. The second method was to manually measure the volume fraction of δ. The volume fraction results could then be compared between the low and acceptable ductility samples and between the two methods.

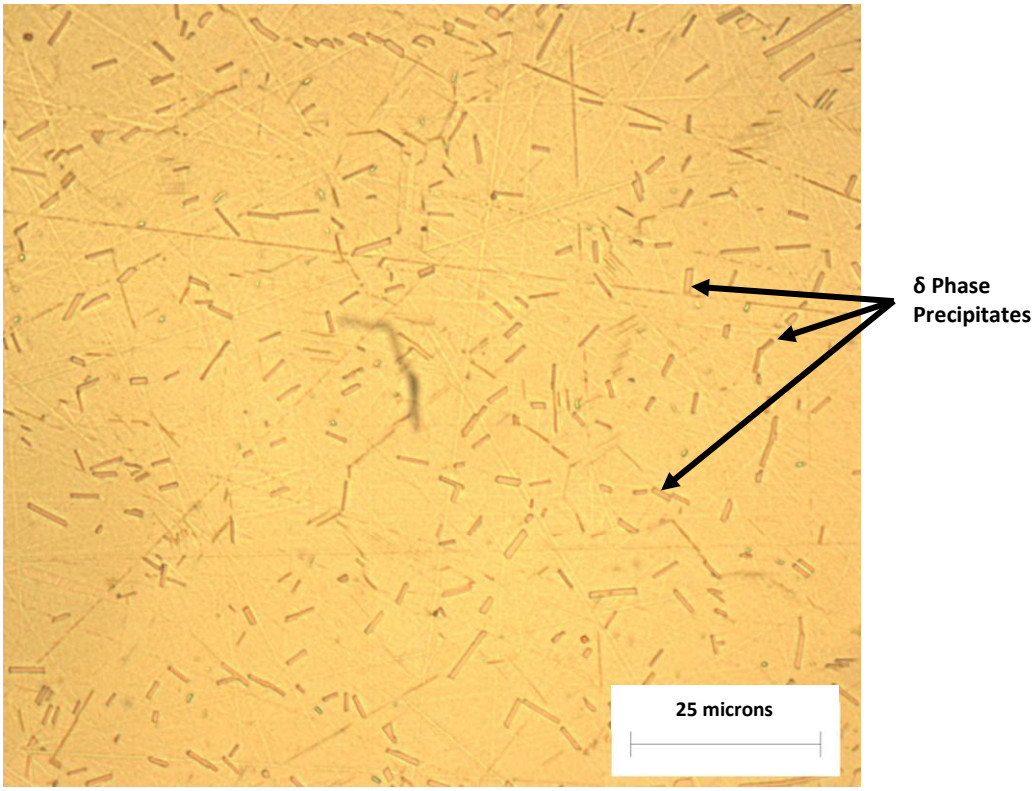

Figure 16. 718 Plus micrograph used for δ phase volume fraction measurements showing δ phase precipitates in the alloy's microstructure. Modified Kalling's, 1000x

Automated Volume Fraction Measurements

The volume fraction of δ was measured in twenty 500x micrographs per sample. Because the δ phase precipitates had a different color and contrast compared to the matrix, the IQM program's detection level could be set to measure δ phase precipitates. Precipitates were highlighted in green to show the operator what phase the program was selecting. The detection level would then be set accordingly to only measure δ phase precipitates. Volume fractions of δ phase could then be measured for each micrograph and then averaged to get the mean volume fraction of δ in each sample. Measurement accuracy using this method was found to be greatly dependent on operator skill and program settings. Volume fraction measurements were sensitive to small adjustments in program settings such as contrast, color level, and intensity. The

high sensitivity and dependence on operator skill using this method can easily cause measurements to be inaccurate. Results obtained from using this method may not give a true representation of actual δ phase volume fractions. To insure accurate volume fraction measurements the second manual method was used to measure volume fraction of δ in each sample.

Manual Volume Fraction Measurements

For manual volume fraction measurements, a systematic point counting procedure was used to measure the volume fraction of δ phase precipitates in each sample. This method was in accordance with ASTM standard E562-11[18]. According to the ASTM standards, the E562-11 method is the most accurate method for measuring volume fraction of a phase, more accurate than the software-based method. To begin, a square ten by ten grid of points was created on a clear plastic transparency sheet (Figure 17). Micrographs used in this method were produced at 1000x magnification so that the average δ phase precipitate size was one half the grid spacing. The 100 point grid was then superimposed into each 718 Plus micrograph. The specified amount of δ present in 718 Plus according to ATI Allvac is between 5 and 10 percent. Based on the expected volume fraction of δ and information in the standard, 64 micrographs per sample were measured to insure at least 10 percent relative accuracy. Volume fraction measurements were conducted by counting the number of test grid points falling inside of a precipitate for each micrograph (P_i). Points that fell on the edge of a precipitate were counted as half. Because a grid of 100 points was used, P_i was equal to the percent of grid points that fell inside of a precipitates ($P_{P(i)}$). $P_{P(i)}$ could then be averaged for the 64 micrographs to get the average volume fraction of δ present in each sample. This method was repeated for all samples and produced a more accurate representation of δ phase volume fractions compared to the automated method.

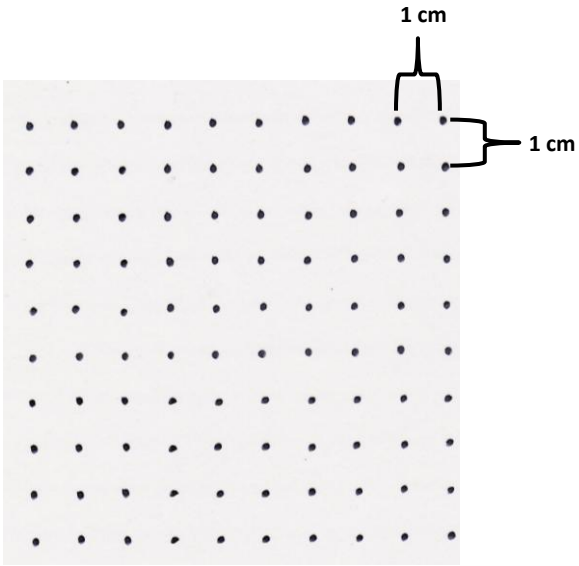

Figure 17. Test grid superimposed over 718 Plus micrographs to measure volume fraction of δ phase precipitates.

Fracture Surface Analysis

Fracture surface analysis was performed on 718 Plus tensile test specimens to compare fracture surface characteristics between low and acceptable ductility specimens (Figure 18). Images of the fracture surfaces were taken using a scanning electron microscope (SEM). Two fracture surfaces were imaged, one from a tensile test specimen with low room temperature ductility and one with acceptable room temperature ductility. The low ductility specimen had an elongation of 13 percent while the acceptable ductility specimen had an elongation of 22 percent. The two tensile test specimens were selected to have

Figure 18. Tensile test specimens of 718 Plus used for fracture surface analysis. Tensile tests were previously conducted by Schlosser Forge.

the greatest difference in ductility. This was to ensure that if differences did exist between the two specimens they would have the highest chance of being observed. SEM images were taken at varying magnifications from 60x to 5000x. Images were then compared to see if any differences in fracture mode existed between the low and acceptable ductility specimens.

Results

Grain Size Results

Grain size results between the automated and manual measurement methods were compared first. A histogram of ASTM grain size numbers measured in all micrographs was created to compare the two methods (Figure 19). The histogram shows an obvious difference in the average grain sizes and grain size distributions between the two methods. The automated method on average measured higher grain sizes in all six samples compared to manual method. The average grain size measured for the automated method was 7.4 (about 27.6 μm grain diameter) and the average for the manual method was 5.8 (about 48.1 μm grain diameter). This large difference can be attributed to the problem encountered with using the IQM program to measure grain size. The program counted δ phase precipitates as grain boundary intersections resulting in higher average ASTM grain size measurements. Because of this problem, grain size results from the automated method were disregarded and attention was focused on the manual results (Table IV). Manual results show grain sizes in all 718 Plus samples ranged between about a 5.5 and 6 ASTM grain size number. Results show no significant difference in grain size between the low and acceptable ductility samples in both the transverse and longitudinal orientations (Figure 20). To support this observation, a series of two sample t-tests were performed to test for equivalence in measured grain sizes between samples (Table V). The t-tests showed no statistical difference exists between the low and acceptable ductility samples or between the two acceptable ductility samples forged at different temperatures. Based on these results it appears that grain size is not contributing to the low room temperature ductility problem.

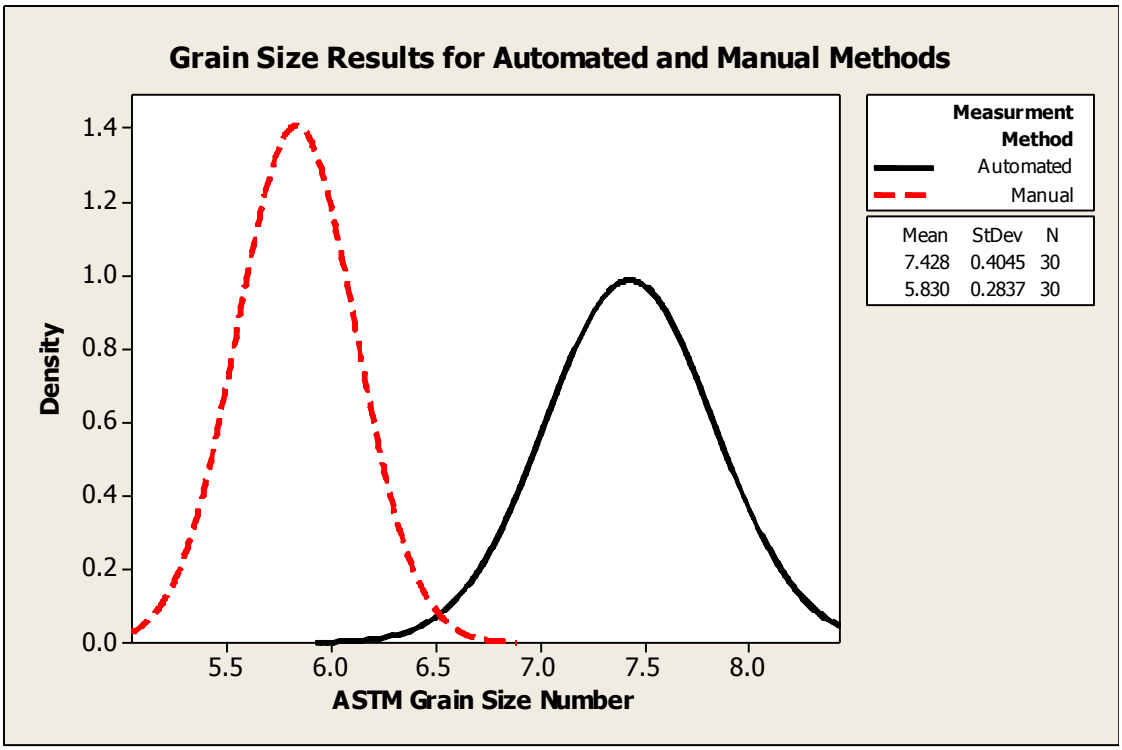

Figure 19. Distributions of measured ASTM grain sizes comparing grain size results from automated and manual methods. Note the automated method measured higher average gain sizes compared to the manual method.

Table IV. Grain Size Results for 718 Plus Forged Samples (Manual Method)

Ductility	Forging Temperature	Orientation in Forged Case	Average ASTM Grain Size Number	Average Grain Diameter (µm)	Standard Deviation
Low	1825°F	Transverse	6.01	44.7	0.1947
		Longitudinal	5.95	45.7	0.1912
Acceptable	1825°F	Transverse	5.75	49.0	0.3475
		Longitudinal	5.57	52.1	0.3832
Acceptable	1850°F	Transverse	5.83	47.6	0.1550
		Longitudinal	5.86	47.1	0.2630

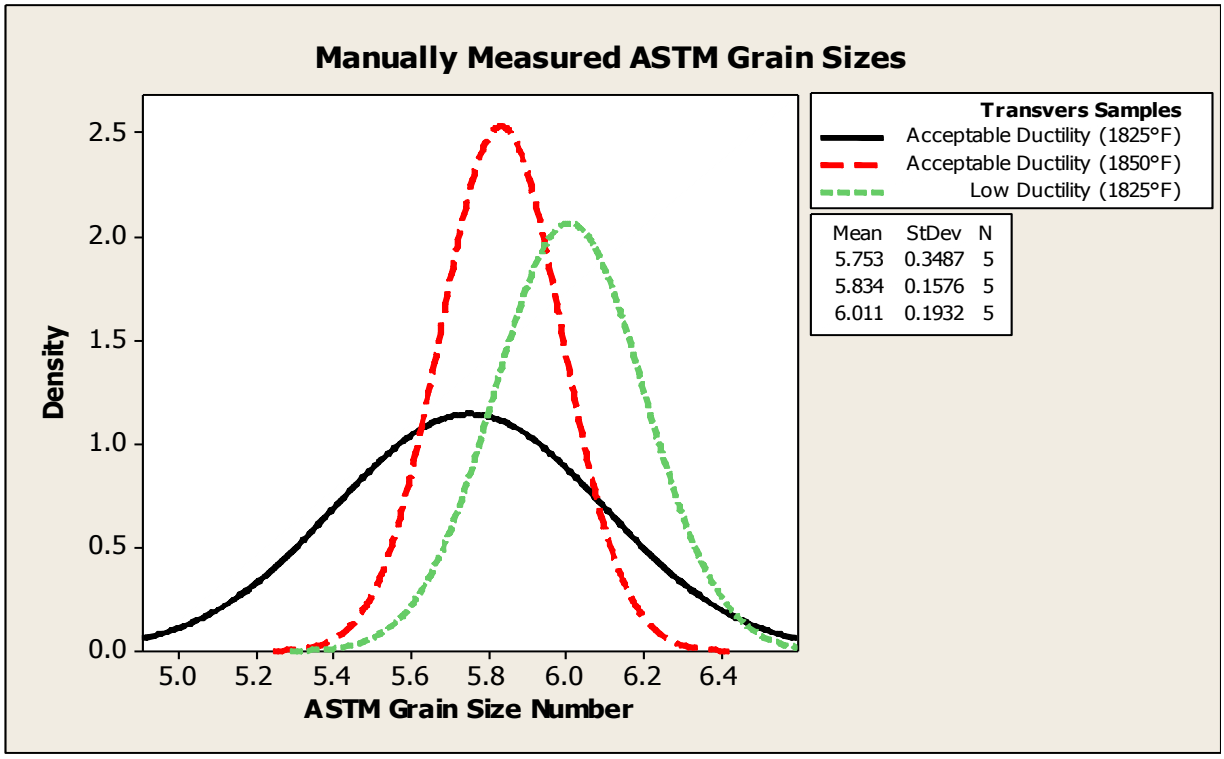

Figure 20. Distributions of manually measured ASTM grain sizes comparing all three transverse 718 Plus forged samples.

Table V. Two Sample t-test Results Comparing Measured Grain Sizes

Sample Orientation	Samples Compared	P-Value	Conclusion with 0.05 α-Level
Transverse	Low Ductility (1825˚F) vs. Acceptable Ductility (1825˚F)	0.198	Equal
	Low Ductility (1825˚F) vs. Acceptable Ductility (1850˚F)	0.157	Equal
	Acceptable Ductility (1825˚F) vs. Acceptable Ductility (1850˚F)	0.654	Equal
Longitudinal	Low Ductility (1825˚F) vs. Acceptable Ductility (1825˚F)	0.107	Equal
	Low Ductility (1825˚F) vs. Acceptable Ductility (1850˚F)	0.573	Equal
	Acceptable Ductility (1825˚F) vs. Acceptable Ductility (1850˚F)	0.207	Equal

Delta Phase Volume Fraction Results

Volume fraction results were analyzed to see if any trends existed between the volume fractions of δ, room temperature ductility, and forging temperature. The first set of data came from the automated method using the IQM program to measure volume fraction of δ (Table VI). The first observation to note is the measured volume fractions of δ in all 718 Plus samples were between 5 and 10 percent, the expected volume fraction range of δ in 718 Plus. The data shows the volume fraction of δ was the same in both the low ductility sample and acceptable ductility sample forged at 1850˚F. The highest amount of δ was measured in the acceptable ductility sample forged at 1825˚F. The automated volume fraction results do not show a relationship between the volume fraction of δ in 718 Plus and room temperature ductility (Figure 21). If a relationship did exist, the amount of δ is expected to be less in samples with acceptable ductility. These results do not support that relationship. The data also does not support the theory that increasing the forging temperature to 1850˚F, just above the δ solvus temperature, reduces the volume fraction of δ. Based on these results, increasing the forging temperature had no effect on reducing the volume fraction of δ. However, these results may not give a true representation of the amounts of δ present in the samples due to the high variability encountered using the automated method. These results will either be supported or disproved by the more accurate systematic point count manual method.

Table VI. Delta Phase Volume Fractions from Automated Method

Ductility	Forging Temperature	Average Volume Fraction of Delta (%)	Standard Deviation
Low	1825°F	6.6 ± 0.4	0.575
Acceptable	1825°F	7.1 ± 0.5	0.757
Acceptable	1850°F	6.6 ± 0.4	0.683

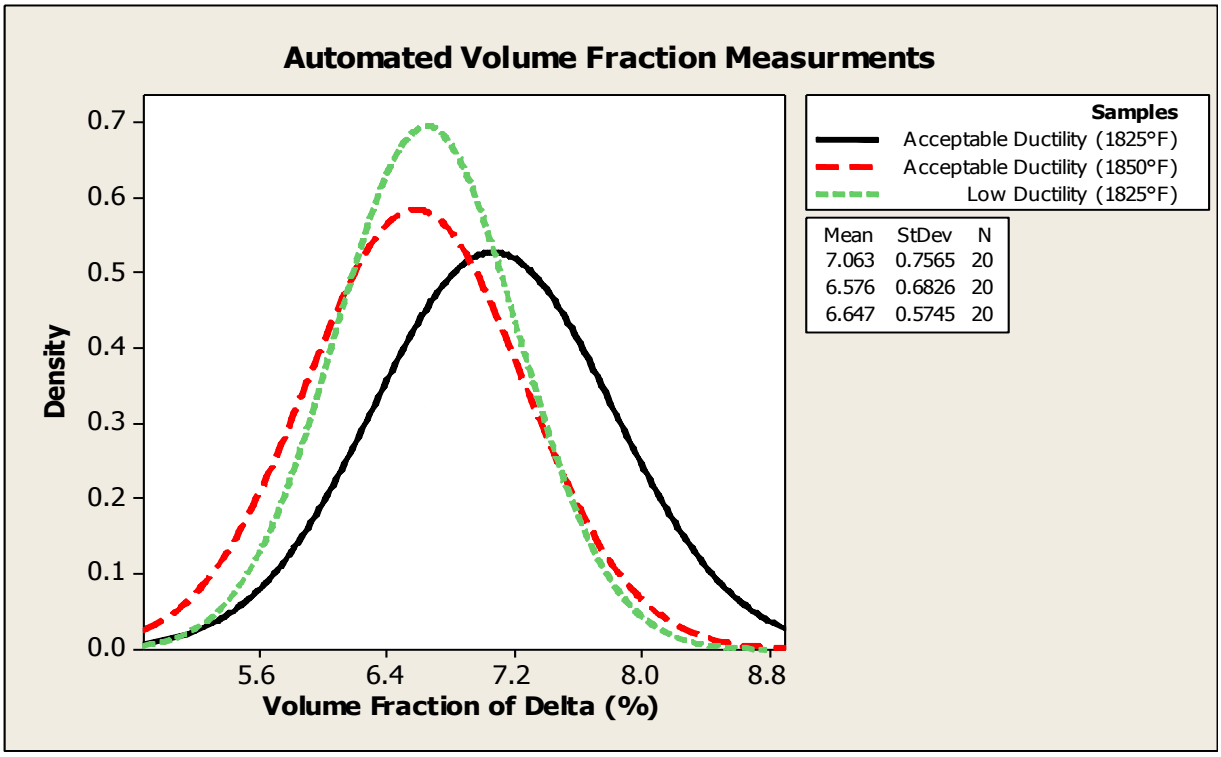

Figure 21. Distributions of δ phase volume fractions comparing the volume fraction of δ in all three 718 Plus samples measured using the automated method.

The manual systematic point count method as specified in ASTM E562-11 provides the most accurate way of measuring the volume fraction of a phase. The results from this method proved to be different from the automated method and relationships could be established between ductility, forging temperature, and volume fraction of δ (Table VII). The first relationship can be established by comparing volume fraction of δ to ductility. The data shows the sample with low ductility contained the most amount of δ, 7.5 percent, while both acceptable ductility samples contained less. The data implies volume fraction of δ in 718 Plus is inversely proportional to ductility at room temperature. The second relationship is drawn from comparing volume fraction of δ to forging temperature. The sample of 718 Plus forged at the higher 1850˚F forging temperature contained the least amount of δ, 4.9 percent, compared to the other two samples forged at the lower temperature. This shows that volume fraction of δ in 718 Plus is also inversely proportional to forging temperature. A distribution plot of δ phase volume fraction results comparing all three samples shows these relationships (Figure 22). In order to support the two

relationships, two sample t-tests were performed on the data to determine whether or not volume fraction of δ was statistically different between samples (Table VIII). Results from the t-test supported both relationships. The volume fraction of δ was found to be statistically different between low and acceptable ductility samples as well as between acceptable ductility samples forged at different temperatures. The results from the systematic point count method disprove the results obtained from the automated method. The systematic point count method is the more accurate method and results should give a more exact representation of the volume fraction of δ in the 718 Plus samples.

Table VII. Delta Phase Volume Fractions from Systematic Point Count Method

Ductility	Forging Temperature	Average Volume Fraction of Delta (%)	Standard Deviation
Low	1825°F	7.5 ± 0.6	2.370
Acceptable	1825°F	6.2 ± 0.6	2.390
Acceptable	1850°F	4.9 ± 0.5	1.901

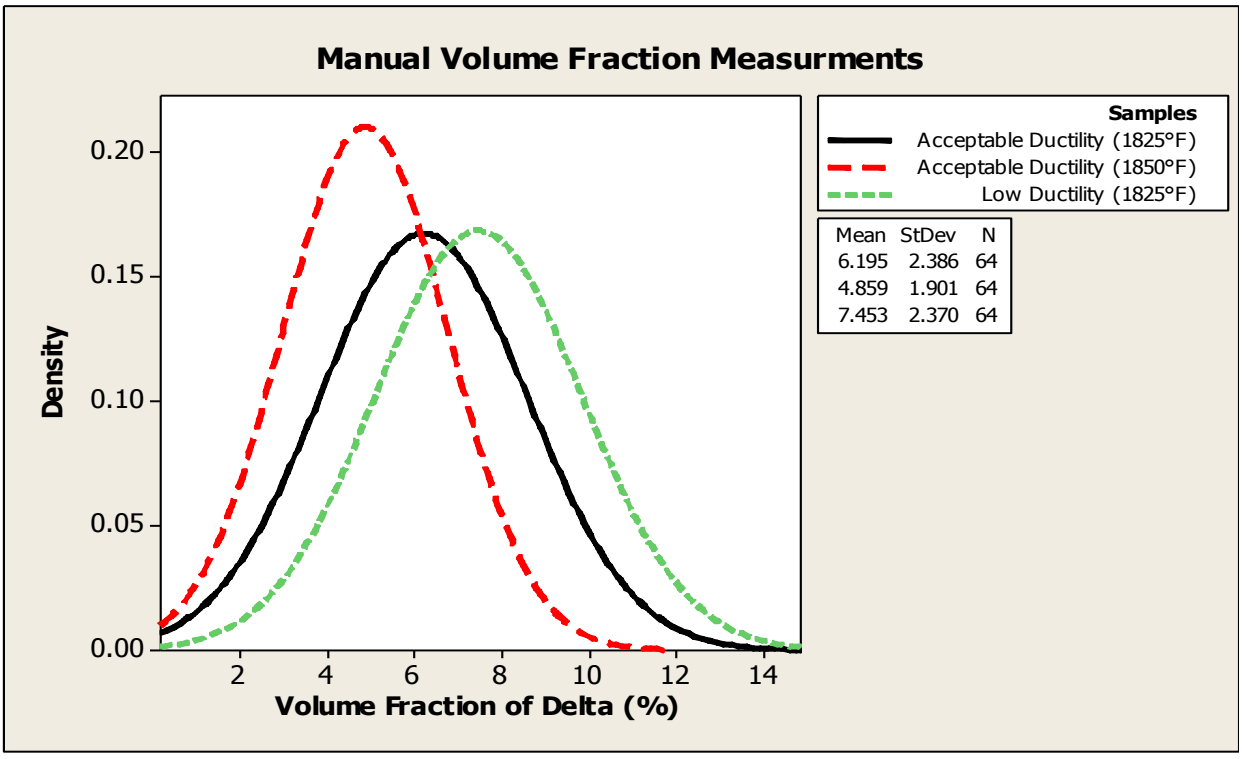

Figure 22. Distributions comparing the manual volume fraction measurements of δ between all three samples. Note less δ is present in samples with acceptable ductility and even less in the sample forged at the higher temperature.

Table VIII. Two Sample t-test Results Comparing Measured Volume Fractions of Delta

Samples Compared	P-Value	Estimated Difference	Conclusion with 0.05 α-Level
Low Ductility (1825˚F) vs. Acceptable Ductility (1825˚F)	0.003	1.285	Not Equal
Low Ductility (1825˚F) vs. Acceptable Ductility (1850˚F)	0.000	2.594	Not Equal
Acceptable Ductility (1825˚F) vs. Acceptable Ductility (1850˚F)	0.001	1.336	Not Equal

Fracture Surface Analysis Results

Fracture surface analysis of 718 Plus tensile test specimens revealed slight differences in fracture surface characteristics between low and acceptable ductility tensile test specimens. The first observation made from the SEM fracture surface images was both low and acceptable ductility specimens showed signs of ductile fracture. The presence of dimples on the fracture surface of both specimens is caused by microvoid coalescence, a ductile fracture mechanism (Figure 23). The main difference between the two specimens is, in additions to dimples, the low ductility specimen also contained regions of brittle cleavage-like features. The brittle cleavage-like regions can be seen as small valleys with smooth sides in the facture surface (Figure 24). Comparing the two specimens, it is evident only the low ductility specimen contained these brittle-like fracture regions and not the acceptable ductility specimen (Figure 25).

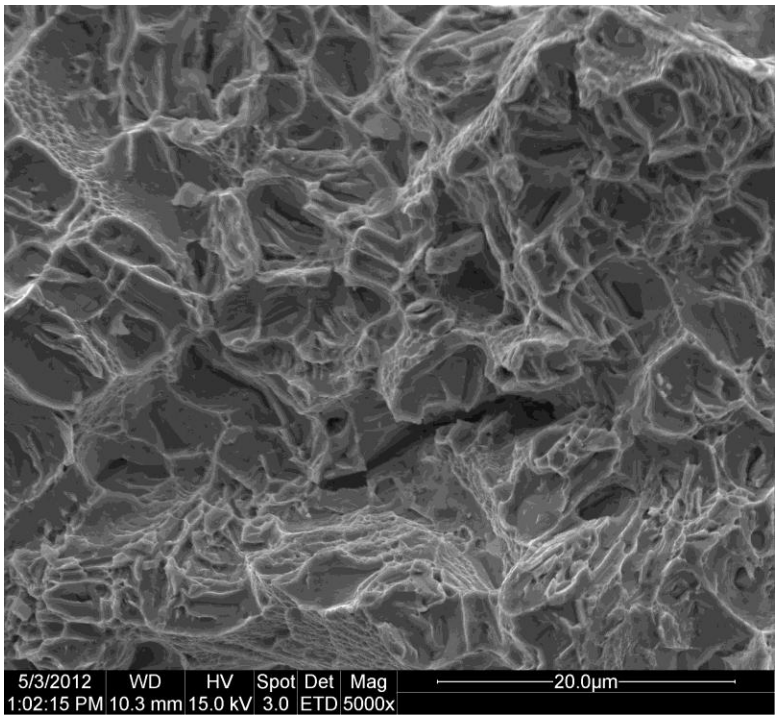

Figure 23. SEM fracture surface image of the acceptable ductility specimen showing dimples caused by microvoid coalescence, a ductile fracture mechanism.

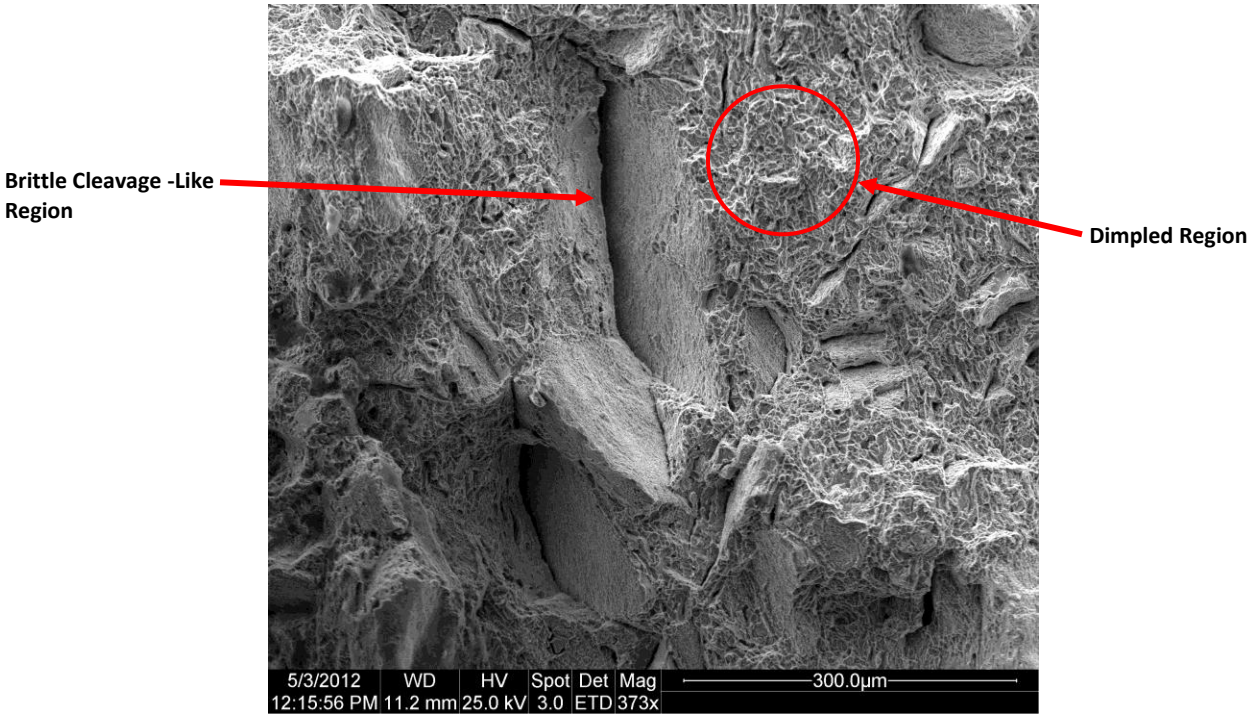

Figure 24. SEM fracture surface image of the low ductility specimen showing dimples as well as brittle cleavage-like regions.

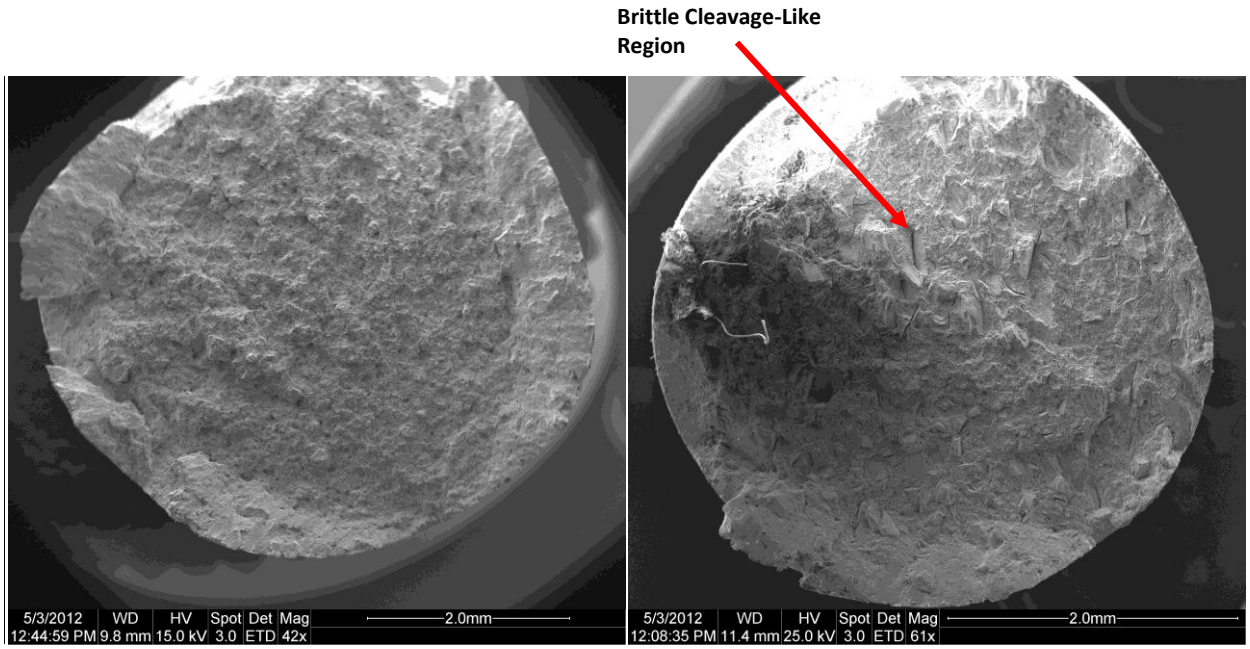

Figure 25. Comparison of SEM fracture surface images of the acceptable ductility (a) and low ductility (b) specimens. Note the presences of brittle cleavage-like regions in the low ductility specimen which are absent in the acceptable ductility specimen.

Discussion

Grain Size

The main objective of this project was to characterize the microstructure of 718 Plus samples and relate those characteristics to the low room temperature ductility problem. Results from the grain size analysis showed that grain size did not differ greatly between low and acceptable ductility samples or between samples with different forging temperatures. Two sample t-tests for equivalency showed grain sizes in all samples tested were statistically equal. Grain size can have a major effect on ductility and strength in alloy systems. In general, smaller more refined grains will result in higher yield strengths and better ductility. Materials with smaller grains will have a larger total grain boundary surface area. The increase in grain boundary surface area will more efficiently impede dislocations and thus increase the strength of the material. The increase in grain boundary area will also increase ductility by providing more locations for dislocations to build up and stresses to be alleviated. If grain size were to effect ductility in 718 Plus LPT cases, it would be expected that grain size would be smaller in samples with acceptable ductility and

larger in samples with lower ductility. However, this was not the case observed in the grain size data. Grain size did not change between low and acceptable ductility samples. It can be concluded that grain size is not affecting the low room temperature ductility problem being experienced in 718 Plus LPT cases.

Volume Fraction of Delta Phase

After analyzing grain size in the 718 Plus samples, volume fraction of δ was addressed next. Schlosser reduced the ductility problem by increasing the forging temperature of their 718 Plus LPT cases to 1850˚F. The significance of increasing forging temperature is now cases are forged just above the solvus temperature of δ, 1830˚F. The theory is by forging above the solvus temperature of δ the amount of δ that precipitates out during the forging process is reduced, thus reducing the total volume fraction of δ in the completed LPT case. The volume fraction data obtained using the systematic point count method supports this theory. Results showed the volume fraction of δ is inversely proportional to forging temperature and room temperature ductility. Forging LPT cases just above the δ solvus temperature reduces the volume fraction of δ in the completed cases, which improves room temperature ductility. It has been experimentally determined that δ phase particles will primarily precipitate out at grain boundaries. Samples of 718 Plus with high amounts of δ will have heavy concentrations of δ phase precipitates along grain boundaries. The high concentration of δ along grain boundaries can prevent grain boundaries from slipping while under stress. This restricts further plastic deformation in the material, effectively reducing ductility. The buildup of δ phase precipitates along grain boundaries may be the mechanism responsible for low room temperature ductility in 718 Plus LPT cases. Another possible mechanism could be that the high concentrations of δ phase precipitates are providing regions for cracks to nucleate and grow. Like most secondary intermetallic phases, δ has a higher hardness than the γ matrix and thus is more brittle. More brittle regions in a material's microstructure serve as a primary location for fractures to occur. Fractures that occur prematurely can restrict a material's ductility and provide another mechanism for low room temperature ductility in 718 Plus LPT cases.

An interesting result seen in the δ phase volume fraction measurements was the difference in the amount of δ present in the two 718 Plus samples forged at 1825°F. This can be attributed to the many variables present in the forging process that effect the precipitation of δ. Of these variables, there are two that could be the primary reason for the observed difference in δ between samples forged at the same temperature. First, the furnaces used in the forging process can vary in temperature from between ±25°F. This variation in furnace temperature could cause certain forging to be at higher or lower temperatures than others. The precipitation of δ in forgings experiencing higher temperatures could be reduced, with the opposite being true for forgings experiencing lower temperatures. This variation in furnace temperature could result in higher or lower volume fractions of δ being present in any one forging. Second, the amount of time spent outside of the furnace can also vary between forgings. Each forging is manipulated by a worker from the furnace into a forging press or machine and then back into the furnace. Certain forgings could be spending more time outside of the furnace than others, causing them to cool to lower temperatures, increasing the precipitation of δ. Again, this could cause a difference in the volume fraction of δ present in any one forging. These effects are magnified in forgings requiring numerous forging steps, such as LPT cases. The average times spent inside and outside of the furnaces will be longer with more forging steps, causing more variation in the volume fractions of δ.

Fracture Surface Characteristics

Fracture surface analysis of the acceptable ductility tensile test specimen concluded ductile fracture to be the primary failure mechanism. This was supported by observing dimples on the fracture surface of the acceptable ductility specimen caused by microvoid coalescence. The formation of microvoids occurs when high stresses cause separation of the base metal around an interface, such as a precipitate. As the stress increases, the microvoids grow and coalesce together to form larger voids. Formation of these large voids eventually causes fracture to occur. In contrast, the low ductility specimen contained a number of smooth cleavage-like surfaces. The cleavage-like surfaces show evidence of brittle fracture occurring in

the low ductility specimen in conjunction with ductile fracture. Brittle fracture usually occurs at flaws in a material where stress concentrations are highest. Cracks normally propagate along the {100} plane. However, cracks can also propagate along grain boundaries, especially when grain boundaries are decorated by a secondary phase. Normally, brittle fracture surfaces are flat and perpendicular to the applied stress direction. The higher volume fraction of δ in the low ductility specimen most likely caused the observed brittle fracture surface features. As mentioned previously, higher volume fractions of δ in 718 Plus will lead to higher concentrations of δ phase precipitates along grain boundaries. Too much δ along grain boundaries can lead to the formation of continuous grain boundary films. The continuous films of δ phase that precipitates along grain boundaries may have initiated brittle intergranular fracture. The smooth brittle fracture surface regions in the low ductility specimen look to be along grain boundaries where concentrations of δ may have been highest. Previous experiments have shown an optimal volume fraction and distribution of δ phase precipitates along grain boundaries exists, providing the best mechanical properties. Exceeding the optimal limit with too much δ could have causes the brittle intergranular fractures which reduced ductility of the specimen. However, no further evidence has been found to support this hypothesis further.

Realistic Constraints

The problem of low room temperature ductility in 718 Plus LPT cases addressed in this project can be related to two realistic constraints: economic and environmental[19]. The first constraint, economics, is perhaps the more obvious of the two. Economics are the driving force behind any company with the bottom line being profitability. It is important for a company like Schlosser Forge to produce quality forgings so the company can remain profitable and competitive in the market[20]. If some of the parts Schlosser manufactures do not meet specific requirements then the part is deemed defective and scraped. Scrapping a part like the LPT case due to low room temperature ductility ends up costing Schlosser

money instead of providing them with a profit. From an economic standpoint, it is critical for Schlosser to solve any problem that affects the quality of their forgings. Failing to produce quality forgings could reduce Schlosser's process capabilities causing them to no longer be competitive in the market. In a worst case scenario Schlosser could be put out of business from losing valuable customers to more competitive forging companies.

The second realistic constraint related to the room temperature ductility problem is environmental. A forging operation consumes large amounts of energy. It is therefore important for a forging company to optimize the efficiency of their forging process to reduce the amount of energy required to forge any one part[21]. In the case of Schlosser, furnaces are used to heat metal ingots to temperatures above 1800˚F during the forging process. Once the forging process is completed, the part is placed in another furnace for a solution treatment and yet another furnace for the final aging. Each furnace runs on natural gas and thus large amounts of fossil fuels are consumed during the forging of a single LPT case. In addition, electricity, most likely generated from fossil fuels, is used during the forging process to power the various presses and ring rolling machines that form the LPT cases into their final shape. Overall, the forging of a single LPT case requires the consumption of large amounts of fossil fuels. If a LPT case fails a specified requirement it is rejected by the customer and has to be recycled. All the energy that went into forging the case is wasted and more energy is now required to recycle the defective case and produce a new one. Fossil fuels are a nonrenewable resource and need to be conserved. The burning of fossil fuels also has a negative effect on the environment due to carbon dioxide emissions. It is important to solve the low room temperature ductility problem in LPT cases to eliminate defective parts and reduce environmental impacts.

Conclusions

1. Grain size in 718 Plus LPT cases did not vary significantly between cases with low room temperature ductility and cases with acceptable room temperature ductility. Grain size also did not differ between LPT cases forged at 1825˚F and cases forged at 1850˚F. Grain size was not a factor contributing to the low room temperature ductility problem.
2. Volume fraction of δ phase precipitates was highest in 718 Plus LPT cases with low room temperature ductility at 7.5 percent by volume. LPT cases with acceptable room temperature ductility forged above the solvus temperature of δ at 1850˚F contained the least amount of δ phase precipitates, 4.9 percent by volume. The volume fraction of δ in 718 Plus is inversely proportional to forging temperature and room temperature ductility and is the primary cause of low room temperature ductility.
3. The fracture mechanism in acceptable ductility 718 Plus tensile test specimens was microvoid coalescence, a ductile fracture mode. In contrast, low ductility specimens contained brittle cleavage-like fracture regions in conjunction with microvoid coalescence. The combination of ductile and brittle fracture mechanisms in 718 Plus can be related to low ductility and high volume fractions of δ phase precipitates.

Acknowledgements

I would like to take the opportunity to thank all the people who contributed to my success on this project. Without their help and guidance this project would have never been possible.

- To Professor Blair London, my advisor, for his superior guidance and support. Your hard work and dedication to my project will never go unforgotten. You have helped me to mature not only as an engineer but as a person. As a result, I have more confidence in myself and my abilities than ever before. Your influence will stay with me forever.
- To Schlosser Forge Co. and Firth Rixson for providing me with such a great opportunity to work on this project.
- To Nathan Lewis at Schlosser Forge for all of his help and support on the project. It has been a pleasure working with you and I have enjoyed every bit of this experience.
- To all of my family and friends for their unwavering support during my college experience.

References

[1] Tien, John K., and Thomas Caulfield. *Superalloys, Supercomposites, and Superceramics*. Boston: Academic, 1989. Print. p 2-3.

[2]Smith, William F. *Structure and Properties of Engineering Alloys*. 2nd ed. New York: McGraw-Hill, 1993. Print. p 504.

[3]Donachie, Matthew J., and Stephen J. Donachie. "Superalloys." *General Background* (2002). *ASM Handbooks Online*. Web. 22 Jan. 2012. <http://http://products.asminternational.org.ezproxy.lib.calpoly.edu/hbk/index.jsp>.

[4]Sims, Chester T., N. S. Stoloff, and William C. Hagel. *Superalloys II*. New York: Wiley, 1987. Print. p 83.

[5]Davis, J. R. *ASM Specialty Handbook: Nickel, Cobalt, and Their Alloys*. Materials Park, OH: ASM International, 2000. Print. p 82.

[6]Donachie, Matthew J., and Stephen J. Donachie. "Superalloys." *Properties and Microstructure* (2002). *ASM Handbooks Online*. Web. 22 Jan. 2012. <http://http://products.asminternational.org.ezproxy.lib.calpoly.edu/hbk/index.jsp>.

[7]Smith, William F. *Structure and Properties of Engineering Alloys*. 2nd ed. New York: McGraw-Hill, 1993. Print. p 506.

[8]Davis, J. R. *ASM Specialty Handbook: Nickel, Cobalt, and Their Alloys*. Materials Park, OH: ASM International, 2000. Print. p 79.

[9]ASTM International. “Standard Test Methods for Determining Averaged Grain Size.” E112-10

[10]Davis, J. R. *ASM Specialty Handbook: Nickel, Cobalt, and Their Alloys*. Materials Park, OH: ASM International, 2000. Print. p 85.

[11]Cao, Wei-Di. "Solidification and Solid State Phase Transformation of Allvac 718 Plus Alloy." *Superalloys 718, 625, 706 and Derivatives Edited by E.A. Loria TMS (The Minerals, Metals & Materials Society)*, 2005 (2005): 165-77. Web. 8 May 2012. <http://www.atimetals.com/products/718Plus-alloy/Documents/165.pdf>.

[12]*ATI 718Plus Alloy Data Sourcebook*. Monroe, NC: ATI Allvac, 2010. Print.

[13]Cemal Kushan, Melih, Sinem Cevik Uzgur, Yagiz Uzunonat, and Fehmi Diltemiz. *ALLVAC 718 Plus™ Superalloy for Aircraft Engine Applications*. Rep. Print.

[14]"The Seamless Rolled Ring Forging Process." *Scot Forge*. Web. 05 Feb. 2012. <http://www.scotforge.com/sf_facts_rollring.htm>.

[15]"Ring Rolling." *Brück*. Web. 05 Feb. 2012. <http://www.bruck.nl/ringrolling/>.

[16]ASTM International. "Standard Guide for Preparation of Metallographic Specimens." E3-11

[17]ASTM International. "Standard Test Method for Determining Average Grain Size Using Semiautomatic and Automatic Image Analysis." E1382-97

[18]ASTM International. "Standard Test Method for Determining Volume Fraction by Systematic Manual Point Count." E562-11

[19]ABET Criteria for Accrediting Engineering Programs 2010-13, General Criteria for Baccalaureate Level Programs, General Criteria 3: Student Outcomes (c), www.abet.org/engineering-criteria-2012-2013.

[20]"Capability Analysis Brought Process into Control, Boosted Quality of Forged Automotive Parts." *FORGING SOLUTIONS Design Engineering Information From FIA* (2007). Web. 08 Apr. 2012. <http://www.forging.org/system/files/field_document/RolledRingCase.pdf>.

[21]United States. U.S. Department of Energy. Energy Efficiency and Renewable Energy. *Forging Facility Uses Plant-Wide Energy Assessment to Aid Conversion to Lean Manufacturing*. Web. 8 Apr. 2012. <http://www1.eere.energy.gov/manufacturing/tech_deployment/pdfs/jernberg_steel_cs.pdf>